Inorganic Chemistry

Article

pubs.acs.org/IC

Luminescence in Phosphine-Stabilized Copper Chalcogenide Cluster Molecules—A Comparative Study

Andreas Eichhöfer,*[,†,∥,⊥] Gernot Buth,[‡] Sergei Lebedkin,[†] Michael Kühn,[§] and Florian Weigend[†,§]

[†]Institut für Nanotechnologie, [‡]ANKA Synchrotronstrahlungsquelle, and [§]Institut für Physikalische Chemie, Abteilung für Theoretische Chemie, Karlsruher Institut für Technologie (KIT), Campus Nord, Hermann-von-Helmholtz-Platz 1, 76344 Eggenstein-Leopoldshafen, Germany

[∥]Lehn Institute of Functional Materials, Sun Yat-Sen University, Guangzhou 510275, China

[⊥]Karlsruhe Nano Micro Facility (KNMF), Hermann-von-Helmholtz-Platz 1, 76344 Eggenstein-Leopoldshafen, Germany

Supporting Information

ABSTRACT: The electronic properties of a series of eight copper chalcogenide clusters including $[Cu_{12}S_6(dpppt)_4]$ (dpppt = $Ph_2P(CH_2)_5PPh_2$), $[Cu_{12}Se_6(dppo)_4]$ (dppo = $Ph_2P(CH_2)_8PPh_2$), $[Cu_{12}S_6(dppf)_4]$ (dppf = $Ph_2PCpFeCpPPh_2$), $[Cu_{12}S_6(PPh_2Et)_8]$, $[Cu_{12}S_6(PEt_3)_8]$, $[Cu_{24}S_{12}(PEt_2Ph)_{12}]$, $[Cu_{20}S_{10}(PPh_3)_8]$, and $[Cu_{20}S_{10}(P^tBu_3)_8]$ were investigated by absorption and photoluminescence (PL) spectroscopy as well as time-dependent density functional theory calculations. Major features of the experimental electronic absorption spectra are generally well-reproduced by the spectra simulated from the calculated singlet transitions. Visualization of the nonrelaxed difference densities indicates that for all compounds transitions at higher energies (above ∼2.5 eV, i.e., below ∼495 nm) predominantly involve excitations of electrons from orbitals of the cluster core to ligand orbitals. Conversely, the natures of the lower-energy transitions are found to be highly sensitive to the specifics of the ligand surface. Bright red PL (centered at ∼650−700 nm) in the solid state at ambient temperature is found for complexes with all '$Cu_{12}S_6$' (E = S, Se) cores as well as the dimeric '$Cu_{24}S_{12}$', although in $[Cu_{12}S_6(dppf)_4]$, the PL appears to be efficiently quenched by the ferrocenyl groups. Of the two isomeric '$Cu_{20}S_{10}$' complexes the prolate cluster $[Cu_{20}S_{10}(PPh_3)_8]$ shows a broad emission that is centered at ∼820 nm, whereas the oblate cluster $[Cu_{20}S_{10}(P^tBu_3)_8]$ displays a relatively weak orange emission at ∼575 nm. The emission of all complexes decays on the time scale of a few microseconds at ambient temperature. A very high photostability is quantitatively estimated for the representative complex $[Cu_{12}S_6(dpppt)_4]$ under anaerobic conditions.

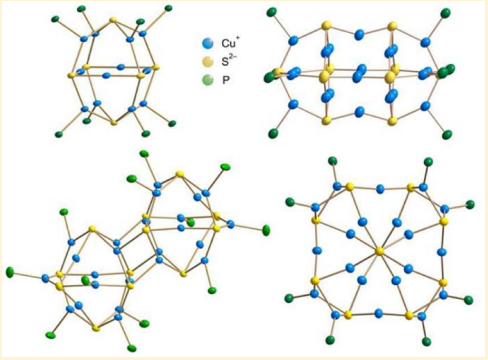

INTRODUCTION

Recently we demonstrated that large polynuclear copper complexes, namely, $[Cu_{12}S_6(dpppt)_4]$ (dpppt = $Ph_2P(CH_2)_5PPh_2$) and $[Cu_{12}S_6(dppo)_4]$ (dppo = $Ph_2P(CH_2)_8PPh_2$), attain photoluminescence (PL) efficiency at ambient temperature as high as >48%.[1] Consequently, these complexes may be a valuable addition to the luminescent mononuclear Cu(I) complexes. The latter display PL quantum yields up to ∼90% in the solid state at ambient temperature and have gained an increasing interest in the last years with regard to their application in organic light emitting diodes.[2,3] The polynuclear copper complexes can possess remarkable structural rigidity, which may be advantageous for photophysical properties, for instance, for photostability or enhanced quantum yields.[4]

In fact, bright-light emission has also been observed, although not quantified in terms of efficiency, for a number of smaller polynuclear Cu(I) complexes like $[Cu_4(\mu_4\text{-}E)(dppm)_4]^{2+}$ (E = S, Se; dppm = bis(diphenylphosphino)methane),[5] $[Cu_6(mtc)_6]$ (mtc$^-$ = di-*n*-propylmonothio-carbamate),[6] $[Cu_6(btt)_6]$ (btt$^-$ = 2-benzothiazolethiolate),[7] $[Cu_3(dppm)_3(\mu_3\text{-}SR)_2]^{+}$[8] and $[Cu_4(p\text{-}S\text{-}C_6H_4NMe_2)_4(dppm)_2]$,[9] which are stabilized by bidentate phosphine ligands.

A large number of phosphine-stabilized Cu(I) chalcogenide clusters that comprise bridging E^{2-} ligands (E = S, Se, and Te) are known.[10,11] In certain cases it was possible to modify the ligand surrounding by keeping the same cluster core structure, whereas in other cases variation of the reaction conditions yielded clusters of different size and structure for the same kind of phosphine ligand. Investigation of such "homologous" complexes is of special interest for elucidating correlations between their structure and photophysical properties. Here we report on a comparative experimental and theoretical investigation of the electronic properties of five copper chalcogenide cluster complexes that share a similar '$Cu_{12}E_6$' (E = S, Se) core stabilized by different phosphine ligands, one complex with the core that can be considered as a '$Cu_{12}S_6$' dimer, and two isomeric '$Cu_{20}S_{10}$' complexes.

Received: May 21, 2015
Published: September 17, 2015

DOI: 10.1021/acs.inorgchem.5b01146
Inorg. Chem. 2015, 54, 9413−9422

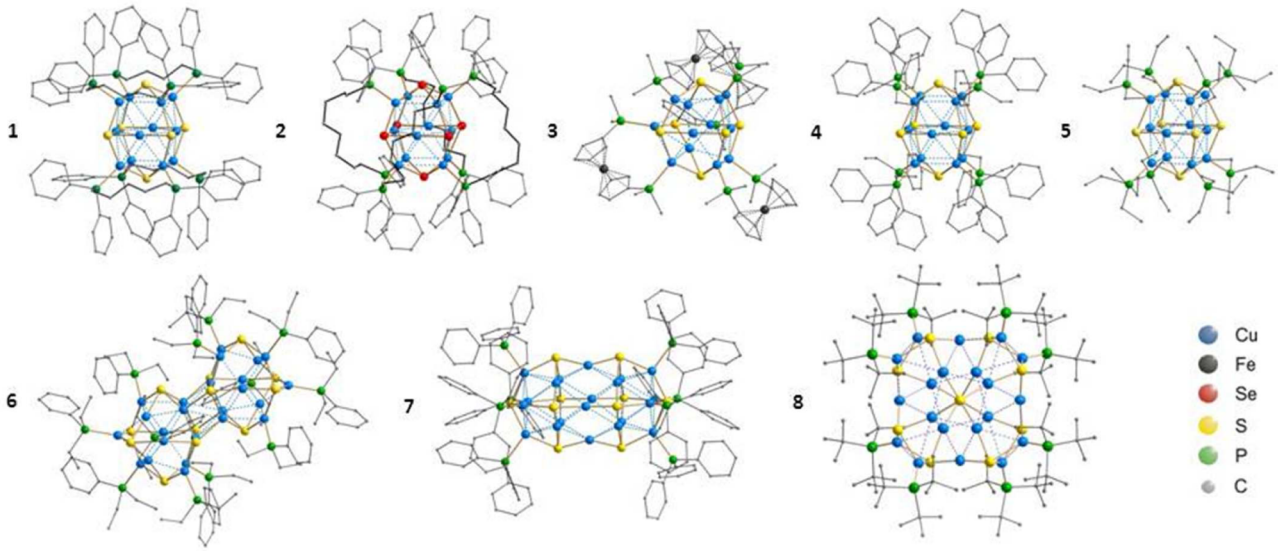

Figure 1. Molecular structures of **1**–**8** (H atoms omitted for clarity). Thermal ellipsoid plots of **1**, **2**, **5a**, **6a**, and **8** can be found in Figures S1–S5 in the Supporting Information. For bond lengths and distances see Table 3; for bond angles see Table S1, Supporting Information.

RESULTS AND DISCUSSION

In this work, the electronic properties of eight copper chalcogenide cluster molecules **1**–**8** (Figure 1, Table 1) were investigated and compared. The synthesis and structural data have already been published for **3**,[12] **4**, **5**, and **7**.[13] Below, we describe the synthesis and structures of the other compounds as well as some further details of the crystallographic analysis of **5**.

Table 1. List of Compounds 1–8

no.	compound
1	$[Cu_{12}S_6(dpppt)_4]$
2	$[Cu_{12}Se_6(dppo)_4]$
3	$[Cu_{12}S_6(dppf)_4]$
4	$[Cu_{12}S_6(PPh_2Et)_8]$
5	$[Cu_{12}S_6(PEt_3)_8]$
6	$[Cu_{24}S_{12}(PEt_2Ph)_{12}]$
7	$[Cu_{20}S_{10}(PPh_3)_8]$
8	$[Cu_{20}S_{10}(P^tBu_3)_8]$

Synthesis and Structure. A bright orange precipitate of crystals of **1** can be obtained by reaction of copper(I) acetate with $S(SiMe_3)_2$ and dpppt in diethyl ether similar to the recently reported synthesis of $[Cu_{12}S_6(dpppt)_4]$[1] in toluene (Scheme 1). In close analogy to the synthesis of $[Cu_{12}S_6(dppo)_4]$,[1] the use of the selenium precursor compound $Se(SiMe_3)_2$ in the reaction with copper(I) acetate and dppo afforded red crystals of $[Cu_{12}Se_6(dppo)_4]$ (**2**) from toluene.

Scheme 1

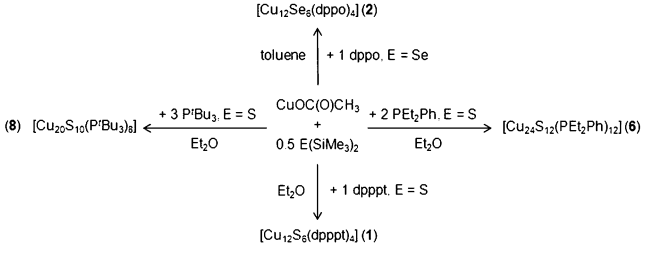

The cluster complexes $[Cu_{12}S_6(dppf)_4]$ (**3**) (dppf = $Ph_2PCpFeCpPPh_2$),[12] $[Cu_{12}S_6(PPh_2Et)_8]$ (**4**), $[Cu_{12}S_6(PEt_3)_8]$ (**5**), and $[Cu_{20}S_{10}(PPh_3)_8]$ (**7**)[13] were synthesized according to the reported procedures (see Experimental Section). The reaction of copper(I) acetate with $S(SiMe_3)_2$ in diethyl ether yields in the presence of PEt_2Ph red crystals of $[Cu_{24}S_{12}(PEt_2Ph)_8]$ (**6**), whereas the use of P^tBu_3 affords orange crystals of $[Cu_{20}S_{10}(P^tBu_3)_8]$ (**8**).

1 crystallizes in the triclinic space group $P\bar{1}$ with the cluster molecule residing on an inversion center. The molecular structure of **1** is isostructural to that reported for the cluster that crystallizes in the tetragonal space group with toluene molecules in the crystal lattice (Table 2, Figure S1, Supporting Information).[1] It can be best described as consisting of an almost ideal octahedron of sulfur atoms with the 12 copper atoms bridging the edges (for a comparison of distances and bond lengths of **1**–**8** see Table 3; for bond angles see Table S1, Supporting Information). The phenyl groups at the phosphine ligands display slightly different orientations in the two different crystal structures, which might be attributable to packing effects.

2 also crystallizes in the triclinic space group $P\bar{1}$ (Table 2). The molecular structure of **2** (Figure S2, Supporting Information) is isostructural to that of the related sulfide cluster $[Cu_{12}S_6(dppo)_4]$,[1] however, with slightly different geometrical parameters (nonbonding Se···Se: 453.7–458.4, Cu–Se: 229.5–245.8, Cu···Cu: 259.0–310.5 pm) due to the different covalent radii of sulfur (103 pm) and selenium (116 pm; Table 3).[14] A similar selenide-bridged '$Cu_{12}Se_6P_8$' cluster core stabilized by monodentate phosphine ligands has been reported before for $[Cu_{12}Se_6(PPh_2Et)_8]$.[13]

Compound **5** crystallizes as previously reported in the triclinic space group $P\bar{1}$ (Table 2).[13] Depending on the measurement temperature we could identify two slightly different unit cells. From room temperature (RT) to 200 K the reflections could be indexed with the triclinic unit cell **5a**, which differs from the reported one by the angle γ (found γ = 87.291(4), reported γ = 78.4(6)°). At 180 K we found a slightly different triclinic unit cell **5b**. Below 180 K the crystals visibly crack and show diffuse diffraction images. Geometrical

DOI: 10.1021/acs.inorgchem.5b01146
Inorg. Chem. 2015, 54, 9413–9422

Table 2. Crystallographic Data for $[Cu_{12}S_6(dpppt)_4]$ (1), $[Cu_{12}Se_6(dppo)_4]$ (2), $[Cu_{12}S_6(PEt_3)_8]$ (5a, 5b), $[Cu_{24}S_{12}(PEt_2Ph)_{12}]$ (6a, 6b), and $[Cu_{20}S_{10}(P^tBu_3)_8]$ (8)

	1	2·4$C_6H_5CH_3$	5a	5b	6a·2$C_2H_5OC_2H_5$	6b	8
sum formula[a]	$C_{116}H_{120}Cu_{12}P_8S_6$	$C_{156}H_{144}Cu_{12}P_8Se_6$	$C_{48}H_{120}Cu_{12}P_8S_6$	$C_{48}H_{120}Cu_{12}P_8S_6$	$C_{128}H_{200}Cu_{24}O_2P_{12}S_{12}$	$C_{120}H_{180}Cu_{24}P_{12}S_{12}$	$C_{96}H_{216}Cu_{20}P_8S_{10}$
fw [g/mol]	2716.71	3502.70	1900.03	1900.03	4052.19	3903.95	3209.85
crystal system	triclinic	triclinic	triclinic	triclinic	triclinic	triclinic	tetragonal
space group	$P\bar{1}$	$P\bar{1}$	$P\bar{1}$	$P\bar{1}$	$P\bar{1}$	$P\bar{1}$	$P4/nnc$
cell a [Å]	13.850(3)	17.944(4)	12.0912(5)	12.335(3)	14.7868(15)	14.807(6)	23.2385
c	14.115(3)	18.566(4)	12.5980(5)	12.251(4)	16.5674(17)	16.715(7)	
b	16.125(3)	23.845(5)	15.0529(6)	15.140(3)	18.3835(19)	18.188(7)	12.7837
α [deg]	67.36(3)	83.60(3)	65.941(3)	65.81(3)	94.796(1)	114.897(4)	
β	72.51(3)	81.32(3)	67.992(3)	65.57(3)	102.005(1)	91.888(4)	
γ	79.80(3)	71.96(3)	87.291(4)	84.91(3)	112.140(1)	110.200(4)	
V [Å^3]	2768.2(12)	7449(3)	1926.04(15)	1891.1(9)	4014.5(7)	3940.2(14)	6903.6(3)
Z	1	2	1	1	1	1	2
T [K]	180(2)	180(2)	200(2)	180(2)	150(2)	150(2)	180(2)
λ [Å]	Mo Kα	Cu Kα	Mo Kα	Mo Kα	0.8000	0.8000	Cu Kα
d_c [g cm^{-3}]	1.630	1.562	1.638	1.668	1.676	1.730	1.544
$\mu(\lambda)$ [mm^{-1}]	2.530	4.666	3.596	3.662	4.784	5.120	5.763
F[000]	1380	3504	972	972	2052	1968	3304
$2\theta_{max}$ [deg]	52	136	52	51	60	54	147
meas reflns	31 269	136 363	18 605	15 152	24 308	23 155	20 383
unique reflns	11 309	10 070	7500	7046	15 907	10 631	3435
R_{int}	0.0557	0.0811	0.0286	0.0579	0.0310	0.0567	0.112
reflns with $I > 2\sigma(I)$	9233	94 138	6416	6027	12 701	8083	2601
refined params	640	1524	341	331	728	659	153
$R1$ $(I > 2\sigma(I))$[b]	0.0337	0.0624	0.0362	0.0309	0.0321	0.0611	0.0437
$wR2$ (all data)[c]	0.0851	0.1710	0.1243	0.0860	0.0786	0.1846	0.1110

[a]No H atoms were calculated on disordered toluene molecules of **2**. [b]$R1 = \sum||F_0| - |F_c||/\sum|F_0|$. [c]$wR2 = \{\sum[w(F_0^2 - F_c^2)^2]/\sum[w(F_0^2)^2]\}^{1/2}$.

DOI: 10.1021/acs.inorgchem.5b01146
Inorg. Chem. 2015, 54, 9413−9422

Table 3. Comparison of Ranges of Atom Distances [pm] in 1−8 (Figure 1)[a]

	E	Cu−E	E···E	Cu···Cu
1	S	215.3−238.4	431.9−440.0	259.8−295.1
2	Se	229.5−245.8	453.7−458.4	259.0−310.5
3	S	218.0−235.6	428.3−437.1	256.1−292.3
4	S	213.6−239.9	430.8−445.0	256.9−296.8
5b	S	215.1−240.4	432.0−443.1	261.2−291.7
6a	S	216.1−240.4	364.6−452.3	259.2−307.6
6b	S	214.4−249.7	366.4−450.4	255.3−314.0
7	S	214.5−235.9	421.2−435.2	263.6−290.0
8	S	215.5−236.0	367.0−462.7	259.4−294.2

[a]Cu···Cu and E···E (E = S, Se) distances considered up to 315 and 500 pm, respectively. Data of **3**,[12] **4**, and **7**[13] were taken from the corresponding literature.

parameters of the '$Cu_{12}S_6P_8$' cluster core of **5a** are now very similar to those of the related cluster $[Cu_{12}S_6(PPh_2Et)_8]$ (**4**) (Table 3, Figure S3, Supporting Information) with no evidence for a tetragonal distortion as discussed in the original paper.[13] In **5a** almost all ethyl groups of the PEt_3 ligands display disorder, which is significantly reduced in the low-temperature form **5b**. The structural transformation of **5a** to **5b** is therefore affected by ordering when cooled. However, the accompanied change of the cell volume induces stress to the crystals as indicated by a poor reversibility and cracking of the crystals below 180 K.

Compound **6** crystallizes in the triclinic space group $P\bar{1}$ as a mixture of crystals with two different unit cells **6a** and **6b**, which differ in their content of lattice solvent molecules (Table 2). The molecular structures of the '$Cu_{24}S_{12}P_{12}$' cluster cores in **6a** and **6b** are identical and possess an inversion center (Figure S4, Supporting Information). They can be formally described as a "dimer" of two strongly distorted '$Cu_{12}S_6P_6$' cluster cores, for example, similar to that in **3**[12] with two phosphine ligands less. An identical cluster core has also been observed in $[Cu_{24}S_{12}(PMe^iPr_2)_{12}]$.[15] When dried (removal of the solvent) **6a** converts to the solvent-free crystal structure of **6b** as can be seen from the respective powder diffraction patterns (Figure S5, Supporting Information).

Compound **8** crystallizes in the tetragonal space group *P*4/*nnc* (Table 2). Although **8** displays the same composition of copper, sulfur, and phosphorus atoms as found in **7**, it forms a molecular structure of a different type. In contrast to the structures of **6** and **7**, the cluster core of **8** has no direct relation to the '$Cu_{12}S_6$' cluster core of **1**−**5** (Figure S6, Supporting Information). Cu−S bond lengths and Cu···Cu distances are quite similar in **7** and **8**, whereas nonbonding S···S distances spread a wider range in **8** than in **7** (Table 3). An identical cluster core to that in **8** has also been observed in $[Cu_{20}S_{10}(P^nBu^tBu_2)_8]$.[16] The cluster complexes **8** and **7** can formally be described as the oblate and prolate isomers of a cluster of composition $[Cu_{20}S_{10}(PR_3)_8]$.

A brief comparison of the molecular structures of **1**−**8** gives the following picture. The '$Cu_{12}E_6P_8$' (E = S, Se) cluster cores of **1**−**5** have an almost similar buildup (Figure 1, Table 3, and Table S1, Supporting Information). They consist of an octahedron of chalcogen atoms (**1**, **2**, **4**, and **5**: S; **2**: Se) with the 12 copper atoms bridging the edges, which itself forms two face-sharing tetragonal antiprisms. In **1**, **2**, **4**, and **5** each copper atom at the upper and lower square planar face of these tetragonal antiprisms is three-coordinated by one phosphorus atom and two chalcogen atoms, whereas the four copper atoms in the middle square planar face have a distorted linear coordination by two chalcogen atoms. In **3** the coordination mode of the respective copper atoms is changed in the way that now two of the bidentate dppf ligands bridge two pairs of copper atoms one at the upper and one at the lower square face. The other two phosphine ligands each bridge a copper atom from the upper/lower and the middle square face. Therefore, two of the eight three-coordinated copper atoms are now situated in the middle square face and two of the four two-coordinated copper atoms in the upper/lower square face leading to a distinct distortion of the ideal '$Cu_{12}E_6P_8$' (E = S, Se) cluster cage found in **1**, **2**, **4**, and **5**.

The cluster molecule in **6** can formally be described as a dimer of two strongly distorted '$Cu_{12}S_6$' cluster cores.[12] Instead of being coordinated by phosphine ligands two of the copper atoms from an upper or lower square of each '$Cu_{12}S_6$' subunit are coordinated by two equatorial sulfur atoms of the other '$Cu_{12}S_6$' subunit, which leads in total to four Cu−S bonds between the two distorted subunits. In addition and similar to **3** two of the phosphine atoms of each '$Cu_{12}S_6P_8$' subunit coordinate to copper atoms in the middle square of copper atoms.

The cluster core of **7** can be considered as a dimer of two "fused", that is, strongly distorted, '$Cu_{12}S_6$' cages.[11,13] Referring to the structural description of **1**, **2**, **4**, and **5** the two subunits are now fused at the top/bottom of the cluster by formal cleavage of eight phosphine ligands, two apical sulfur atoms, and one Cu_4 face. In this way the 10 sulfur atoms form a bicapped tetragonal prism with the copper atoms bridging all edges. The cluster core of **8** has no direct relation to the '$Cu_{12}S_6$' cluster cores of **1**−**7**. The respective S_{10} polyhedron can be described as a highly compressed tetragonal antiprism with the copper atoms bridging edges resulting in 12 copper atoms with a distorted linear coordination by two sulfur atoms and 12 copper atoms, which are three-coordinate by two sulfur and one phosphorus atom.

Cu−S, Cu···Cu, and S···S bond lengths and distances are almost similar in **1** and **3**−**8** but, as expected, increased in the selenide-bridged cluster **2** (Table 3). For compounds **6a**, **6b**, and **8** the range of nonbonding S···S distances extends to smaller values than in the other copper sulfide cluster molecules.

The measured powder patterns of **1**−**8** show a good agreement with the calculated ones based on the single-crystal data (Figures S5 and S7−S13, Supporting Information), and thus prove the crystalline purity of the compounds.

Comparison of Measured and Calculated Electronic Absorption Spectra. Absorption spectra were measured in a region within 300−800 nm (4.13−1.55 eV) for powdered crystals of **1**−**8** in mineral oil layer between two quartz plates (Figure 2). They were compared with the singlet transition peaks calculated with time-dependent density functional theory (TDDFT) employing the Becke−Perdew functional (BP86) and polarized split valence basis sets (def2-SV(P)).[17] From these transitions the experimental spectra were simulated by superimposing Gaussians with a full width at half-maximum (fwhm) of 0.3 eV. The spectra were shifted by 0.75 eV, according to our previous results.[1] It has been shown that for this class of compounds BP86[18] reproduces well the peak positions calculated with the much more time-consuming B3-LYP functional[19] (Becke's three-parameter hybrid functional with Lee−Yang−Parr correlation) as well as the peak positions

DOI: 10.1021/acs.inorgchem.5b01146
Inorg. Chem. 2015, 54, 9413−9422

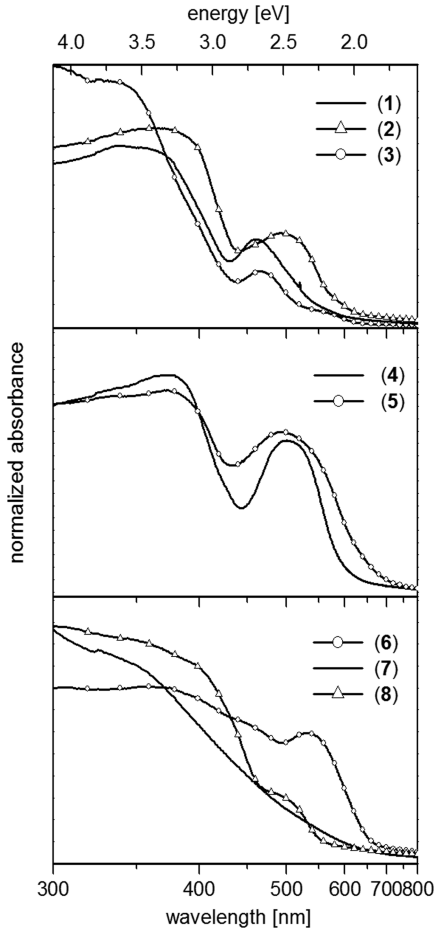

Figure 2. Electronic spectra of **1**–**8** measured as powdered crystals in mineral oil.

from the experiment—apart from the above-mentioned overall shift. Figures 3a,c (**4**–**6**), 4a,b (**7**–**8**), and S14–S16 (**1**–**3**) demonstrate a similarly good agreement between the calculated and measured spectra. For instance, the experimental spectra of compounds **1**–**6** show a single peak between 2.8 and 2.0 eV (443 and 620 nm), which is well-reproduced by the simulated spectra (with the only exception of **1**). The absorption profiles of **8** and **7**, displaying a shoulder and a featureless onset of the absorption, are also in agreement with the calculations.

Visualization of the nonrelaxed difference densities (see ref 1), as illustrated for selected transitions in **1**–**8** in Figures 3, 4, and S14–S16, indicates that all transitions at energies higher than ∼2.5 eV predominantly involve excitations of electrons from orbitals of the cluster core to ligand orbitals. In **1**, **3**, **6**, and **7**, this is also the case for all transitions at lower energies. In **3**, the electron is not only transferred to the phenyl rings of the phosphine ligands but also to a significant degree to Fe d-orbitals of the $FeCp_2$ moiety. In contrast, the lowest-energy transitions in **2**, **4**, **5**, and **8** involve also transitions within the copper chalcogenide cluster core, which are particularly dominant for the "phenyl-free" clusters **5** and **8**. In these cases electron density is preferably transferred from the filled copper d-orbitals (43%–50%) and sulfur p-orbitals (12%–28%) to the empty orbitals of copper atoms (mainly p, 24%–57%), which are coordinated by the phosphine ligands. The numbers in parentheses result from Mulliken analyses for the respective peaks of compounds **2**, **4**, **5**, and **8**.

In general the character of the low-energy transitions is very sensitive to changes in the phosphine ligand sphere. For example **1** and **4** differ only in the fact that the phosphine ligands in **1** are bidentate, whereas in **4** they are monodentate. The structural buildup of the two cluster cores including bond lengths and angles is very similar (Table 3 and Table S1, Supporting Information); nevertheless, the character of the excitation band is different (significant transfer of electrons within the '$Cu_{12}S_6$' cluster core for **4** but not for **1**). We

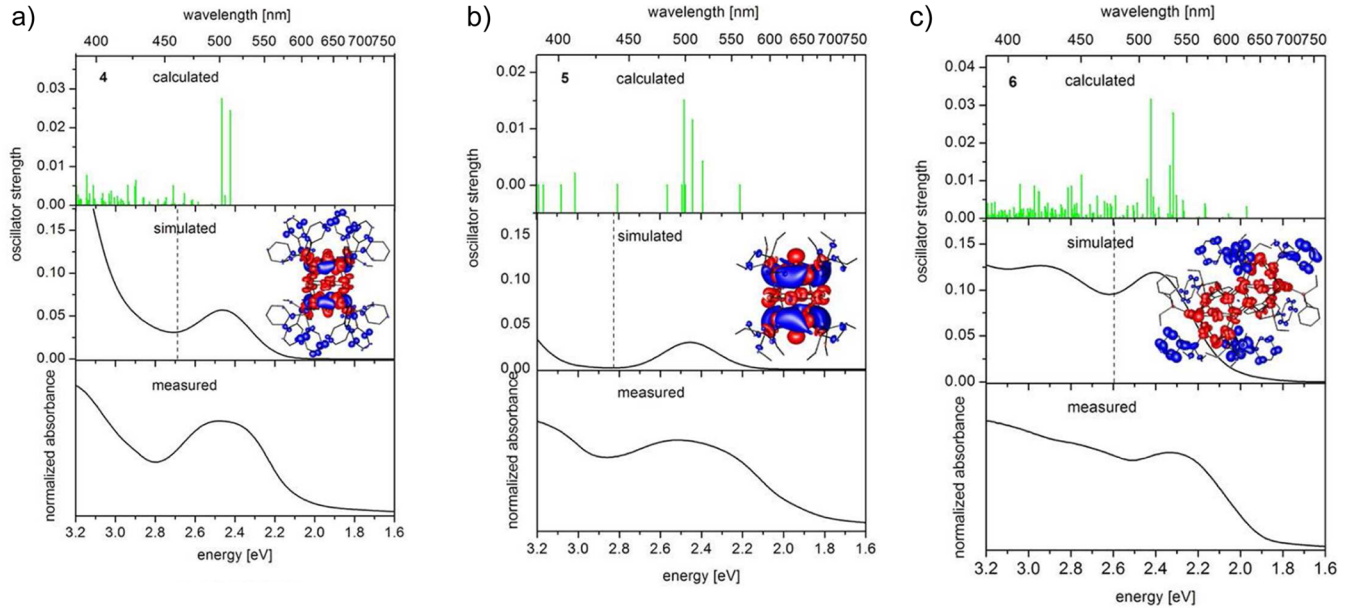

Figure 3. Comparison of measured electronic spectra (powdered crystals in mineral oil) of (a) **4**, (b) **5**, and (c) **6** with calculated singlet excitation energies and oscillator strengths plotted as vertical lines (green) as well as by superimposed Gaussians of fwhm = 0.3 eV (black) to simulate the experimental spectrum. The character of the peaks (up to 2.67 eV in **4**, 2.82 eV in **5**, and 2.60 eV in **6**) was visualized using the nonrelaxed difference densities (see Experimental Section). The contributions of occupied orbitals are plotted in red, and those of the unoccupied orbitals are in blue.

DOI: 10.1021/acs.inorgchem.5b01146
Inorg. Chem. 2015, 54, 9413–9422

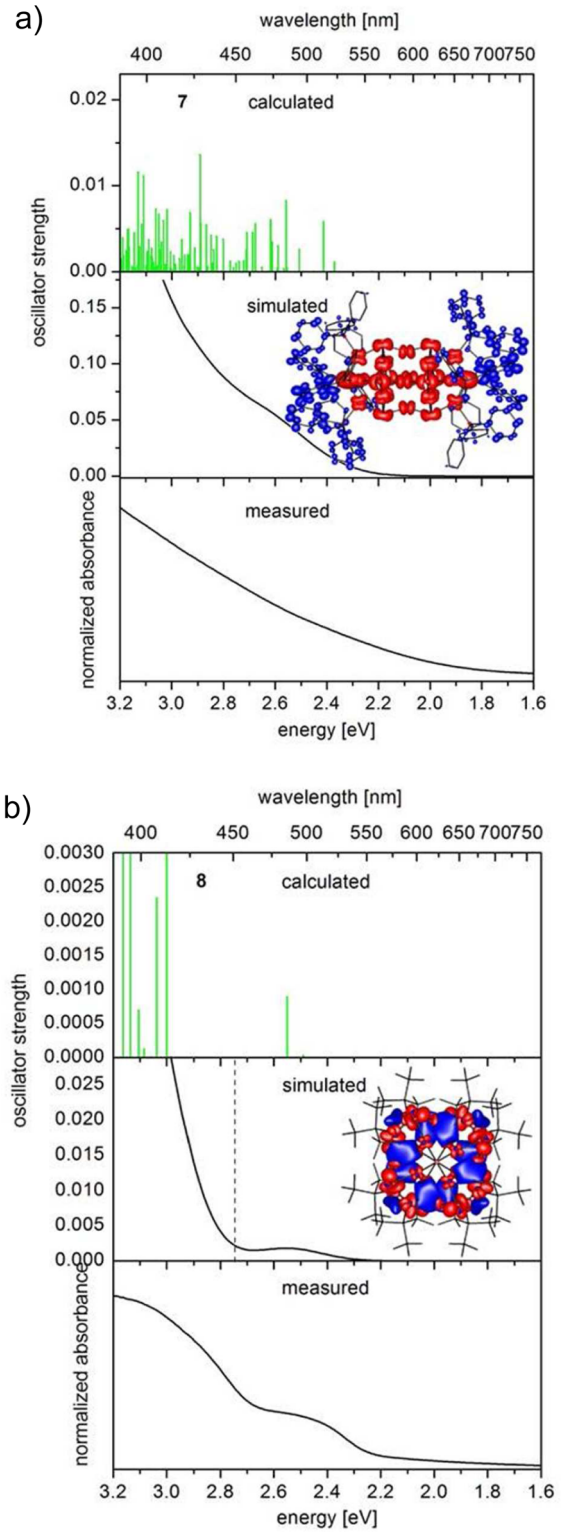

Figure 4. Comparison of measured electronic spectra (powdered crystals in mineral oil) of (a) **7** and (b) **8** with calculated singlet excitation energies and oscillator strengths plotted as vertical lines (green) as well as by superimposed Gaussians of fwhm = 0.3 eV (black) to simulate the experimental spectrum. The character of the peaks (up to 2.67 eV in **8**) was visualized using the nonrelaxed diffference densities (see Experimental Section). The contributions of occupied orbitals are plotted in red, and those of the unoccupied orbitals are in blue.

investigate this in detail now. In both cases the lowest unoccupied molecular orbital (LUMO) has contributions from the copper orbitals of ca. 15%, according to a Mulliken analysis; the highest occupied molecular orbitals (HOMOs) mainly consist of d(Cu) and p(S) orbitals. For both **1** and **4** the lowest excitation is mainly HOMO → LUMO; the second-lowest is HOMO−1 → LUMO, and the third-lowest is HOMO−2 → LUMO. Relevant for the different character of the excitation band are the oscillator strengths for the second and the third transition (corresponding to peak height and thus used for weighting in the difference density plots of the band), which are more than 10 times higher for **4** than for **1**, 0.03 versus 0.002. The oscillator strength of the lowest transition is negligible (1×10^{-11}) for both cases; it thus does not significantly influence the electron transfer within this band. Obviously the kind of ligand bridging has distinct influence on the distribution of electron density over the cluster upon excitation suggested by distinct differences in the oscillator strengths of similar transitions in similar types of clusters (e.g., **1** and **4**). Having this in mind it is not surprising that their energetic positions display no clear correlation with the cluster size (at least in this size regime).

Photoluminescence Spectra. Bright-red PL in the solid state at ambient temperature appears to be typical for complexes with a '$Cu_{12}E_6$' (E = S, Se) core moiety. In **1**, **2**, **4**, and **5** this PL peaked at ~615−700 nm (Figures 5, 6, S17) and decayed on the time scale of a few microseconds at ambient temperature (i.e., the emission is phosphorescence). The above complexes show high PL quantum yields φ_{PL} between 21 and 63% (Table 4). The emission intensity further increases by decreasing the temperature, thus approaching φ_{PL}

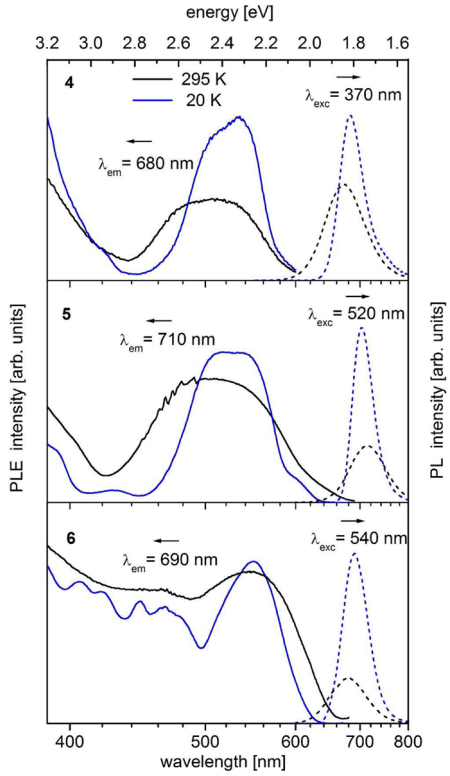

Figure 5. Photoluminescence excitation (PLE, solid line) and emission (PL, dashed line) spectra (powdered crystals in mineral oil) of **4**−**6** at 295 and 20 K, respectively.

DOI: 10.1021/acs.inorgchem.5b01146
Inorg. Chem. 2015, 54, 9413−9422

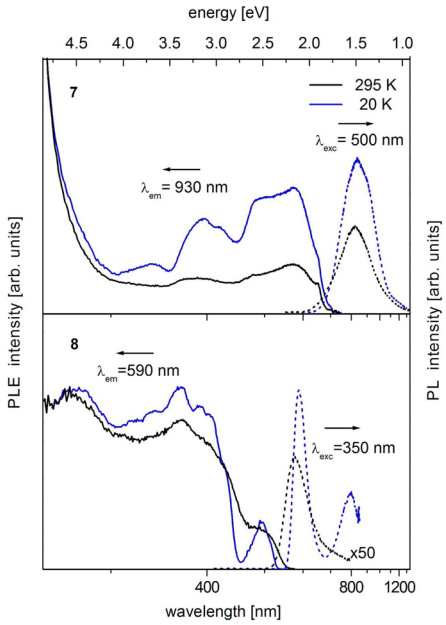

Figure 6. Photoluminescence excitation (PLE, solid line) and emission (PL, dashed line) spectra of **7** and **8** (powdered crystals in mineral oil) at 295 and 20 K, respectively.

Table 4. Photoluminescence Wavelength λ_{PL} [nm] at 295 and 20 K and Corresponding Excitation Wavelength λ_{exc} [nm], Quantum Yield Φ_{PL} [%] at 295 K, and Decay Times τ [μs] for 1−8

compound	λ_{PL}, 295 K	λ_{PL}, 20 K	λ_{exc}	Φ_{PL}, 295 K	τ, 295 K	τ, 20K
1	615	615/712	470	63	τ_1 = 0.96, τ_2 = 5	τ_1 = 2.8, τ_2 = 20/ τ_1 = 143,τ_2 = 34
2	638	638	350	53	5.26	102
3	*a*	636	475	*a*	*a*	*a*
4	673	683	370	45	τ_1 = 0.73, τ_2 = 4	τ_1 = 3, τ_2 = 20 (14 K)
5	713	703	500	21	3.05	12.9
6	680	690	540	39	1.45	160
7	823	842	500	*a*	τ_1 = 0.27, τ_2 = 1.55	*a*
8	575	587/795	350	*a*	*a*	τ_1 = 300, τ_2 = 72/τ_1 = 800, τ_2 = 170

[a]Not measured.

≈ 100% below T ≈ 100 K. Interestingly, the PL decays relatively slowly at cryogenic temperatures, on the time scale up to hundreds of microseconds (Table 4). In other words, PL efficiency does not linearly correlate with the PL lifetime. These common PL properties have also been found for the '$Cu_{12}S_6$' complexes described in ref 1. In detail, however, the luminescence can be significantly affected by the ligands and even crystal packing. This is especially highlighted by a comparison of the isostructural complexes $[Cu_{12}S_6(dpppt)_4]$ that form either triclinic crystals without solvent molecules (**1** in this work) or tetragonal crystals with intercalation of two solvent (toluene) molecules per cluster.[1] The triclinic and tetragonal polymorphs display at ambient temperature red emission at 615 versus 648 nm with biexponential (τ_1 = 0.96 μs and τ_2 = 5.0 μs) versus monoexponential (τ = 6.1 μs)[1] decay behavior, respectively. Another evidence for the influence of the crystal packing is the PL broadening and variation of the decay parameters for the vacuum-dried tetragonal crystals, whereas the PL of the (solvent-free) triclinic form is not affected. At low temperatures, in contrast to the tetragonal polymorph, the triclinic form demonstrates a second minor emission band at ∼710 nm (Figure S17). It demonstrates a particularly slow decay on the time scale of hundreds of microseconds (Table 4).

The (minor) differences in the PL properties of **1**, **2**, **4**, and **5** may also be attributed to the effects of different ligand shells and crystal packing. Note that the latter result into slightly but notably varying atom−atom distances in the cluster cores of the above compounds (Table 3). Correspondingly, the ligands and crystal packing may also affect the electronic transitions within the cluster core.

In contrast to other '$Cu_{12}E_6$' complexes, $[Cu_{12}S_6(dppf)_4]$ (**3**) emits very weak red PL even at cryogenic temperatures (Figure S18). The reason is apparently the efficient quenching of electronic excitations both in the ligands and the cluster core via ferrocenyl groups in **3**. The (residual) core emission at ∼640 nm is reduced in **3** by a factor of ∼1×10^5.

Despite the dimeric nature of the cluster core of **6**, accompanied by significant variations in the atom−atom distances, the PL of **6** at ∼680 nm is very similar to that of the "monomeric" compounds **1**, **2**, **4**, and **5** (Figure 5, Table 4). The dimeric complex also demonstrates a high PL quantum yield of 39%. These observations likely indicate the "robustness" of the electronic properties of the '$Cu_{12}E_6$' core against even rather large geometrical distortions (**6** vs **1**, **2**, **4**, and **5**).

The cluster core of **7** can be considered as a dimer of two fused, that is, strongly distorted, '$Cu_{12}S_6$' cages. The solid dimeric complex emits broad near-infrared PL centered at ∼820 nm and extended to ∼1200 nm (Figure 6). Its intensity is substantially lower at ambient temperature than that of the "usual" '$Cu_{12}E_6$' complexes. The PL decays biexponentially on the time scale of a few and hundreds of microseconds at 295 and 20 K, respectively (Table 4).

Despite similar E^{2-} bridging, the '$Cu_{20}S_{10}$' core of **8** is structurally distinct in comparison to **1**−**7**. Also distinct are the PL properties of **8**. The solid complex shows relatively *weak orange* emission at ∼575 nm, which gains in intensity and shifts to ∼590 nm by decreasing the temperature to 20 K (Figure 6, Table 4). Similar to **1**, the low-temperature emission is dual, with a second band at ∼800 nm. The excitation (PLE) spectra of the both bands practically coincide (Figure S19, Supporting Information). For complex **8** the second band demonstrates a slower decay on the time scale of hundreds of microsecond at 20 K (Table 4). The origin of the dual low-temperature emission in **1** and **8** is presently not clear.

For all complexes studied in this work, the PLE spectra well correspond to the absorption spectra discussed above. Relatively small Stokes shifts in the emission suggest only moderate distortions in the excited versus ground states. Note that the sharper and more structured PLE features observed at low temperatures—for example, distinct low-energy peaks in the PLE spectra of **2**, **4**, and **5**—further support the theoretical results (cf. Figures 3, 5, S15, and S17).

Finally, we would like to remark on a generally high photostability of polynuclear copper chalcogenide complexes, in particular, under anaerobic conditions. This valuable property has previously been mentioned but not quantified yet. In this work, it was probed for **1**, one of the most photostable compounds among the highly luminescent '$Cu_{12}E_6$' complexes. Figure S20 in the Supporting Information illustrates

DOI: 10.1021/acs.inorgchem.5b01146
Inorg. Chem. 2015, 54, 9413−9422

a time dependence of the PL intensity of **1** (powdered sample in mineral oil placed into an evacuated cryostat chamber; see Experimental Section) under continuous 60 mW laser irradiation at 457 nm and ambient temperature. According to a rough estimate using the exctinction coefficient of ~10.000 M^{-1} cm^{-1}, sample density of ~1 g/cm^3, ~4 mm^2 irradiation area, and ~80% laser beam absorbance, the observed 10% decrease of the PL intensity after 2 h of laser irradiation (Figure S20, Supporting Information) corresponds to ~1 × 10^5 photons absorbed per molecule of **1**. Such photostability is superior/somewhat inferior to that of pyrromethene/rhodamine 6G laser dyes in sol−gel matrices, that is, under protection against oxygen (in a solution, the photostability of laser dyes decreases dramatically).[20]

CONCLUSIONS

The comparison of the experimental absorption spectra of the copper chalcogenide cluster complexes $[Cu_{12}S_6(dpppt)_4]$, $[Cu_{12}Se_6(dppo)_4]$, $[Cu_{12}S_6(dppf)_4]$, $[Cu_{12}S_6(PPh_2Et)_8]$, $[Cu_{12}S_6(PEt_3)_8]$, $[Cu_{24}S_{12}(PEt_2Ph)_{12}]$, $[Cu_{20}S_{10}(PPh_3)_8]$, and $[Cu_{20}S_{10}(P^tBu_3)_8]$ with the spectra simulated from the calculated singlet transitions (TDDFT) reveals a good overall agreement. The TDDFT method is apparently capable to well reproduce the electronic absorption spectra of these (and likely other) copper cluster complexes. Visualization of the non-relaxed difference densities of the peaks indicates a distinct influence of the kind of the ligand on the character of the lowest-energy transitions. For clusters with low-lying empty ligand π-orbitals, that is, with phenyl groups at the phosphine ligands as found in $[Cu_{12}S_6(dpppt)_4]$, $[Cu_{12}S_6(dppf)_4]$, $[Cu_{24}S_{12}(PEt_2Ph)_{12}]$, and $[Cu_{20}S_{10}(PPh_3)_8]$, excitations mainly involve transitions from orbitals of the cluster core to ligand orbitals. In contrast, for $[Cu_{12}S_6(PEt_{3)8}]$ and $[Cu_{20}S_{10}(P^tBu_3)_8]$, they are dominated by transitions within the copper chalcogenide cluster core.

Bright-red, microseconds-long phosphorescence in the solid state at ambient temperature appears to be characteristic for complexes with a '$Cu_{12}E_6$' (E = S, Se) core. Relatively small Stokes shifts in the excitation and emission spectra suggest moderate distortions in the excited-state geometry. The PL efficiency of 21−63% was found for compounds **1**, **2**, **4**, and **5**. The absence of emission in **3** is due to the quenching effect of ferrocenyl groups and indicates a possibility of efficient energy transfer to/from a copper cluster core. Despite some cluster cage distortion, the bright-red PL (φ_{PL} = 39%) is retained in the cluster dimer $[Cu_{24}S_{12}(PEt_2Ph)_{12}]$. However, the two isomeric structures $[Cu_{20}S_{10}(PPh_3)_8]$ and $[Cu_{20}S_{10}(P^tBu_3)_8]$, which can be considered as strongly "distorted" if referenced to **1**−**6**, demonstrate quite different PL properties than **1**−**6**. By a closer look, the emission properties of homologous '$Cu_{12}E_6$' complexes can also be affected by the kind of phosphine ligands and geometry of the copper chalcogenide cluster. Even the crystal packing can have a notable effect on the emission wavelength, efficiency, and decay parameters. These effects may be used to "adjust" to a certain extent the PL properties of '$Cu_{12}E_6$' complexes.

A practically important photophysical property of copper chalcogenide cluster complexes is their generally high photostability, at least under anaerobic conditions. A first quantitative estimate of the emission stability of the complex $[Cu_{12}S_6(dpppt)_4]$ under prolonged and intense laser irradiation at 457 nm demonstrates that the photostability is comparable to that of the pyrromethene and rhodamine laser dyes.

EXPERIMENTAL SECTION

Synthesis. Standard Schlenk techniques were employed throughout the syntheses using a double manifold vacuum line with high-purity dry nitrogen (99.9994%) and an MBraun glovebox with high-purity dry argon (99.9990%). The solvents diethyl ether (Et_2O), tetrahydrofuran (THF), and toluene were dried over sodium−benzophenone and distilled under nitrogen. $CuOC(O)CH_3$,[21] $S(SiMe_3)_2$,[22] PPh_2Et, PEt_2Ph, PEt_3,[23] and dppo were prepared according to literature procedures. Bis(diphenylphosphinoferrocene (dppf) and bis(diphenylphosphino)pentane (dpppt) were used as received from Sigma-Aldrich.

*$[Cu_{12}S_6(dpppt)_4]$ (**1**).* Dpppt (0.45 g, 1.02 mmol) and $CuOC(O)CH_3$ (0.125 g, 1.02 mmol) were suspended in 40 mL of Et_2O. Addition of P^nBu_3 (0.23 mL, 1.02 mmol) resulted in the formation of an almost clear colorless solution. $S(SiMe_3)_2$ (0.11 mL, 0.51 mmol) was then added at 0 °C, and after one night in the fridge at +2 °C bright orange crystals of **1** had formed. After they warmed to room temperature (RT), the crystals were collected and washed two times with 10 mL of Et_2O to give a final yield of 0.180 g (78.0%).

$C_{116}H_{120}Cu_{12}P_8S_6$ (2716.9). Calcd C 51.3, H 4.5, S 7.1; found C 51.6, H 4.6, S 6.6%. The enhanced experimental values for C and H (reduced for S) are indicative for remaining lattice solvent molecules ($C_{116}H_{120}Cu_{12}P_8S_6$*$C_4H_{10}O$ (2791.1): calcd C 51.6, H 4.7, S 6.9). The single-crystal X-ray analysis also reveals the exsistence of solvent-accessible voids although no such molecules could be localized in the difference Fourier map.

*$[Cu_{12}Se_6(dppo)_4]$ (**2**).* Dppo (0.244 g, 0.5 mmol) and $CuOC(O)CH_3$ (0.062 g, 0.5 mmol) were dissolved in 15 mL of toluene. $Se(SiMe_3)_2$ (0.056 mL, 0.25 mmol) was then added at 0 °C to yield a clear red solution. Then after storing at −27 °C overnight red crystals of **2** appeared. After 3 d they were collected and washed with toluene to give a final yield of 0.094 mg (71%).

$C_{128}H_{144}Cu_{12}P_8Se_6$ (3166.65). Calcd C 48.6; H 4.6 found; C 48.1; H 4.2%.

*$[Cu_{12}S_6(dppf)_4]$ (**3**).* Synthesized according to the literature procedure.[12]

*$[Cu_{12}S_6(PPh_2Et)_8]$ (**4**).* PPh_2Et (1.3 mL, 6.12 mmol) was added to a suspension of $CuOC(O)CH_3$ (0.25 g, 2.04 mmol) in diethyl ether (10 mL) resulting in a clear solution. $S(SiMe_3)_2$ (0.22 mL, 1.02 mmol) was then added at −40 °C to yield a clear colorless solution. Then, after they warmed to +2 °C overnight pink crystals of **4** appeared, which were collected and washed two times with 10 mL of Et_2O after 3 d to give a final yield of 0.307 g (67.6%).

$C_{112}H_{120}Cu_{12}P_8S_6$ (2668.9). Calcd C 50.4, H 4.5, S 7.2; found C 50.2, H 4.1, S 6.8%.

*$[Cu_{12}S_6(PEt_3)_8]$ (**5**).* PEt_3 (0.82 mL, 5.5 mmol) was added to a suspension of $CuOC(O)CH_3$ (0.225 g, 1.84 mmol) in diethyl ether (20 mL) resulting in a clear solution. $S(SiMe_3)_2$ (0.2 mL, 0.92 mmol) was then added at −50 °C. Then, after they warmed to −2 °C dark red crystals of **5** appeared within a few days with a final total yield of 0.230 g (79%).

$C_{48}H_{120}Cu_{12}P_8S_6$ (1900.19). Calcd C 30.3, H 6.4, S 10.1; found C 29.8, H 6.3, S 10.5%.

*$[Cu_{24}S_{12}(PEt_2Ph)_{12}]$ (**6**).* PEt_2Ph (0.9 mL, 4.9 mmol) was added to a suspension of $CuOC(O)CH_3$ (0.3 g, 2.45 mmol) in diethyl ether (20 mL) resulting in a clear solution. $S(SiMe_3)_2$ (0.26 mL, 1.22 mmol) was then added at −40 °C, and the solution was stored at −25 °C overnight. After 1 d red crystals of **6** had grown from a red solution. During 3 d the reaction solution was warmed stepwise to −5 °C; the crystals were then collected and washed three times with cold (−70 °C) Et_2O to give a final yield of 0.242 g (61%).

$C_{120}H_{180}Cu_{24}P_{12}S_{12}$ (3904.28). Calcd C 36.9, H 4.7, S 9.9; found C 36.6, H 4.6, S 9.9%.

*$[Cu_{20}S_{10}(PPh_3)_8]$ (**7**).* PPh_3 (1.29 g, 4.9 mmol) and $CuOC(O)CH_3$ (0.115 g, 1.224 mmol) were dissolved in 25 mL of THF. $S(SiMe_3)_2$ (0.13 mL, 0.612 mmol) was then added at −60 °C, and the solution was allowed to warm to −10 °C. After 7 d orange crystals of **7** were collected and washed at −70 °C once with THF and two times with a 1:1 mixture of THF and Et_2O to give a total yield of 0.47 g (42%).

DOI: 10.1021/acs.inorgchem.5b01146
Inorg. Chem. 2015, 54, 9413−9422

$C_{144}H_{120}Cu_{20}P_8S_{10}$ *(3689.85)*. Calcd 46.9, H 3.3, S 8.7 found; C 46.8, H, 3.2, S 8.4%.

*$[Cu_{20}S_{10}(P^tBu_3)_8]$ (**8**)*. P^tBu_3 (1.6 mL, 6.6 mmol) was added to a suspension of $CuOC(O)CH_3$ (0.27 g, 2.2 mmol) in diethyl ether (40 mL) resulting in a clear solution. $S(SiMe_3)_2$ (0.23 mL, 1.1 mmol) was then added at −20 °C, and the solution was stored at −10 °C overnight. Orange crystals of **8** started to grow from a yellow solution. The reaction solution was allowed to warm to 0 °C. After 3 d the crystals were collected and washed three times with Et_2O to give a final yield of 0.237 g (58.4%).

$C_{96}H_{216}Cu_{20}P_8S_{10}$ *(3210.08)*. Calcd C 35.9, H 6.8, S 10.0; found C 35.9, H 7.0, S 9.5%

Crystallography. Crystals suitable for single-crystal X-ray diffraction were selected in perfluoroalkylether oil and mounted to the diffractometer equipped with an Oxford Cryosystem.

Single-crystal X-ray diffraction data of **2** and **8** were collected using Cu radiation (λ = 1.541 86 Å) generated by a multilayer optic, and those of **5a** were collected using Mo radiation (λ = 0.710 73 Å) generated by a multilayer optic on a STOE STADI Vari (Pilatus Hybrid Pixel Detector 300 K). Single-crystal X-ray diffraction data of **1** and **5b** were collected using graphite-monochromatised Mo Kα radiation (λ = 0.710 73 Å) on a STOE IPDS 2T (Imaging Plate Diffraction System). Raw intensity data of **1**, **2**, and **5** were collected and treated with the STOE X-Area software Version 1.64. Interframe Scaling of the STADI Vari data set of **1** was done with the implemented program LANA. Data were corrected for Lorentz and polarization effects. On the basis of a crystal description a numerical absorption correction was applied for **1**, **2**, **5a**, **5b**, and **8**.[24]

Single-crystal X-ray diffraction data of **6a** and **6b** were measured on the SCD beamline at the ANKA synchrotron (KIT) with a Bruker SMART Apex CCD area detector (λ = 0.80 Å). Raw intensity data were collected and treated with the APEX2 software program package.[25] Data for all compounds were corrected for Lorentz and polarization effects. Multiscan absorption corrections were applied for **6a** and **6b** with the implemented program SADABS.

All structures were solved with the direct methods program SHELXS of the SHELXTL PC suite programs[26] and were refined with the use of the full-matrix least-squares program SHELXL. Data of **2** were refined as a nonmerohedral two-component twin in the HKLF5 format by the implemented twin-refinement method.[27,28] Atomic form factors for λ = 0.800 00 Å (15.466 keV) were obtained by the method of Brennan and Cowan[29] as implemented on http://skuld.bmsc.washington.edu/scatter/AS_periodic.html.

Several tested tiny crystals of **6b** display considerable reflections ($I/\sigma > 10$) only up to 2θ 40° although measured with the high-intensity beam at the synchrotron source. For reflections with a resolution smaller than d = 0.93 Å the mean I/σ ratio drops below 4.4 accompanied by an increase of the R(int) and $R(\sigma)$ values above 0.1794 and 0.1966, respectively. Molecular diagrams were prepared using Diamond.[30]

In **1**, **2**, **5a**, **5b**, **6a**, **6b**, and **8** all Cu, Se, S, P, and C atoms were refined with anisotropic displacement parameters, while H atoms were computed and refined, using a riding model, with an isotropic temperature factor equal to 1.2 times the equivalent temperature factor of the atom that they are linked to. In **2**, solvent C atoms of toluene molecules were partially refined with a split model of site disorder and isotropic displacement parameters. Because of the disorder, C−C distances and C−C−C angles partially differ from the expected ideal values of 139.5 pm and 120°; no H atoms were computed. In **5a** and **5b**, C atoms of disordered ethyl groups as well as of disordered phenyl and ethyl groups in **6a** and **6b** were refined with a split model of site disorder with isotropic displacement parameters. Although the crystal structure of **8** comprises voids of 267 Å^3 no solvent lattice molecules or significant residual electron density (the highest difference peak 0.605, the deepest hole −0.539), respectively, could be identified in the difference Fourier map. Additional crystallographic information can be found in the Supporting Information.

X-ray powder diffraction patterns (XRD) for **1**−**8** were measured on a STOE STADI P diffractometer (Cu Kα1 radiation, Germanium monochromator, Debye−Scherrer geometry, Mythen 1K detector) in sealed glass capillaries both as a suspension of crystals in the mother liquor and as a powder of crystals. The theoretical powder diffraction patterns were calculated on the basis of the atom coordinates obtained from single-crystal X-ray analysis by using the program package STOE WinXPOW.[31]

Physical Measurements. C, H, and S elemental analyses were performed on an Elementar vario Micro cube instrument.

UV−vis absorption spectra were measured on a PerkinElmer Lambda 900 spectrophotometer. Solid-state spectra were measured in transmission for samples that were prepared as micron-sized crystalline powders dispersed in a mineral oil layer between two quartz plates. These were placed in front of a Labsphere integrating sphere.

The PL measurements were performed on a Horiba JobinYvon Fluorolog-3 spectrometer equipped with an optical close-cycle cryostat (Leybold) for measurements at cryogenic temperatures down to 16 K. The emission spectra were corrected for the wavelength-dependent response of the spectrometer and detector (in relative photon flux units). Emission decay traces were recorded by connecting a detector (photomultiplier) to an oscilloscope and using a N_2 laser for pulsed excitation at 337 nm (~2 ns, ~5 μJ per pulse). PL quantum yields φ_{PL} were measured at ambient temperature using a 10 cm integrating sphere out of optical PTFE with low autoluminescence (Berghof GmbH), which was installed in the sample chamber of the Fluorolog-3. Powdered samples between quartz plates were placed into the sphere and excited at 500 nm. The φ_{PL} values were determined according to the method of de Mello et al.[32] The accuracy of their determination was estimated to be ±10%.

Quantum Chemical Treatments. All calculations were performed with Turbomole.[17] The spectra in the paper were obtained at level BP86[18]/def2-SV(P)[33] for the structure parameters of the X-ray structure analysis using TDDFT. The electronic spectrum and the (nonrelaxed) difference densities for a group of transitions forming a peak were visualized at essentially no extra computational effort using the Python script PANAMA (Peak ANAlyzing MAchine).[1]

■ ASSOCIATED CONTENT

Supporting Information

The Supporting Information is available free of charge on the ACS Publications website at DOI: 10.1021/acs.inorgchem.5b01146. CCDC 1044372 (**1**), 1044373 (**2**), 1044374 (**5a**), 1044375 (**5b**), 1044376 (**6a**), 1044377 (**6b**), and 1044378 (**8**) contain the supplementary crystallographic data for this paper. These data can be obtained free of charge at www.ccdc.cam.ac.uk/conts/retrieving.html (or from the Cambridge Crystallographic Data Centre, 12 Union Road, Cambridge CB2 1EZ, U.K.; fax: (internat.) +44−1223/336−033; E-mail: deposit@ccdc.cam.ac.uk).

Molecular structures of **1**, **2**, **5a**, **6a**, and **8**, measured and simulated X-ray powder patterns of **1**−**8**, comparison of measured and calculated electronic spectra of **1**−**3**, steady-state PL excitation and emission spectra of **1**−**3**, **8**, and photostability text of **1**. (PDF)

X-ray crystallographic information for **1**, **2**·4$C_6H_5CH_3$, **5a**, **5b**, **6a**·2$C_2H_5OC_2H_5$, **6b**, and **8**. (CIF)

■ AUTHOR INFORMATION

Corresponding Author

*Phone: 49-(0)721-608-26371. Fax: 49-(0)721-608-26368. E-mail: andreas.eichhoefer@kit.edu.

Notes

The authors declare no competing financial interest.

DOI: 10.1021/acs.inorgchem.5b01146
Inorg. Chem. 2015, 54, 9413−9422

■ ACKNOWLEDGMENTS

This work was supported by the Karlsruhe Institut für Technologie (KIT, Campus Nord). The authors wish to thank S. Stahl for performing the elemental analysis.

■ REFERENCES

(1) Yang, X.-X.; Issac, I.; Lebedkin, S.; Kühn, M.; Weigend, F.; Fenske, D.; Fuhr, O.; Eichhöfer, A. *Chem. Commun.* **2014**, *50*, 11043−11045.
(2) Bergmann, L.; Friedrichs, J.; Mydlak, M.; Baumann, T.; Nieger, M.; Bräse, S. *Chem. Commun.* **2013**, *49*, 6501−6503.
(3) Igawa, S.; Hashimoto, M.; Kawata, I.; Yashima, M.; Hoshino, M.; Osawa, M. *J. Mater. Chem. C* **2013**, *1*, 542−551.
(4) Yersin, H.; Rausch, A. F.; Czerwieniec, R.; Hofbeck, T.; Fischer, T. *Coord. Chem. Rev.* **2011**, *255*, 2622−2652.
(5) Yam, V. W.-W.; Lo, K. K.-W.; Fung, W. K.-M.; Wang, C.-R. *Coord. Chem. Rev.* **1998**, *171*, 17−41.
(6) Ford, P. C.; Vogler, A. *Acc. Chem. Res.* **1993**, *26*, 220−226.
(7) Yue, C.; Yan, C.; Feng, R.; Wu, M.; Chen, L.; Jiang, F.; Hong, M. *Inorg. Chem.* **2009**, *48*, 2873−2879.
(8) Yam, V. W.-W.; Lam, C.-H.; Fung, W. K.-M.; Cheung, K.-K. *Inorg. Chem.* **2001**, *40*, 3435−3442.
(9) Langer, R.; Yadav, M.; Weinert, B.; Fenske, D.; Fuhr, O. *Eur. J. Inorg. Chem.* **2013**, *2013*, 3623−3631.
(10) Fuhr, O.; Dehnen, S.; Fenske, D. *Chem. Soc. Rev.* **2013**, *42*, 1871−1906.
(11) Dehnen, S.; Eichhöfer, A.; Fenske, D. *Eur. J. Inorg. Chem.* **2002**, *2002*, 279−317.
(12) Khadka, C. B.; Najafabadi, B. K.; Hesari, M.; Workentin, M. S.; Corrigan, J. F. *Inorg. Chem.* **2013**, *52*, 6798−6805.
(13) Dehnen, S.; Schäfer, A.; Fenske, D.; Ahlrichs, R. *Angew. Chem., Int. Ed. Engl.* **1994**, *33*, 746−750.
(14) Pyykkö, P.; Atsumi, M. *Chem. - Eur. J.* **2009**, *15*, 186−197.
(15) Dehnen, S.; Fenske, D. *Chem. - Eur. J.* **1996**, *2*, 1407−1416.
(16) Dehnen, S.; Fenske, D.; Deveson, A. C. *J. Cluster Sci.* **1996**, *7*, 351−369.
(17) *Turbomole,* Version 6.5; Turbomole GmbH: Karlsruhe, Germany, 2013. Turbomole is a development of the University of Karlsruhe and the Forschungszentrum Karlsruhe 1989−2007.
(18) (a) Becke, A. D. *Phys. Rev. A: At., Mol., Opt. Phys.* **1988**, *38*, 3098−3100. (b) Perdew, J. P. *Phys. Rev. B: Condens. Matter Mater. Phys.* **1986**, *33*, 8822−8824.
(19) (a) Lee, C.; Yang, W.; Parr, R. G. *Phys. Rev. B: Condens. Matter Mater. Phys.* **1988**, *37*, 785−789. (b) Becke, A. D. *J. Chem. Phys.* **1993**, *98*, 5648−5652.
(20) Dubois, A.; Canva, M.; Brun, A.; Chaput, F.; Boilot, J.-P. *Appl. Opt.* **1996**, *35*, 3193−3199.
(21) Edwards, D. A.; Richards, R. *J. Chem. Soc., Dalton Trans.* **1973**, 2463−2468.
(22) Schmidt, H.; Ruf, H. *Z. Anorg. Allg. Chem.* **1963**, *321*, 270−273.
(23) (a) Sasse, K. In *Methoden der Organischen Chemie (Houben−Weyl);* Sasse, K., Muller, E., Eds.; Georg Thieme Verlag: Stuttgart, Germany, 1963; p 32. (b) Kaesz, H. D.; Stone, F. G. *J. Org. Chem.* **1959**, *24*, 635−637.
(24) *X-RED32 1.01,* Data Reduction Program; STOE & CIE GmbH: Darmstadt, Germany, 2001.
(25) *APEX2 1.22;* Bruker AXS Inc.: Madison, WI, 2005.
(26) Sheldrick, G. M. *SHELXTL 6.14,* An Integrated System for Solving, Refining, and Displaying Crystal Structures from Diffraction Data, Bruker Analytical X-ray Systems; BrukerAXS Inc.: Madison, WI, 2003.
(27) Pratt, C. S.; Coyle, B. A.; Ibers, J. A. *J. Chem. Soc. A* **1971**, 2146−2151.
(28) Jameson, G. B.; Schneider, R.; Dubler, E.; Oswald, H. R. *Acta Crystallogr., Sect. B: Struct. Crystallogr. Cryst. Chem.* **1982**, *B38*, 3016−3020.
(29) Brennan, S.; Cowan, P. L. *Rev. Sci. Instrum.* **1992**, *63*, 850−853.
(30) *Diamond Version 2.1d;* Crystal Impact GbR: Bonn, Germany, 2000.
(31) *STOE WinXPOW;* STOE & Cie GmbH: Darmstadt, Germany, 2000.
(32) de Mello, J. C.; Wittmann, H. F.; Friend, R. H. *Adv. Mater.* **1997**, *9*, 230−232.
(33) Weigend, F.; Ahlrichs, R. *Phys. Chem. Chem. Phys.* **2005**, *7*, 3297−3305.

DOI: 10.1021/acs.inorgchem.5b01146
Inorg. Chem. 2015, 54, 9413−9422